



Amarillo National Resource Center for Plutonium

A Higher Education Consortium of The Texas A&M University System,
Texas Tech University, and The University of Texas System

Gallium Interactions with Zircaloy Cladding

May 1998

This report was prepared with the support of the U.S. Department of Energy (DOE) Cooperative Agreement No. DE-FC04-95AL85832. However, any opinions, findings, conclusions, or recommendations expressed herein are those of the author(s) and do not necessarily reflect the views of DOE. This work was conducted through the Amarillo National Resource Center for Plutonium.

600 South Tyler • Suite 800 • Amarillo, TX 79101
(806) 376-5533 • Fax: (806) 376-5561
<http://www.pu.org>

AMARILLO NATIONAL RESOURCE CENTER FOR PLUTONIUM/
A HIGHER EDUCATION CONSORTIUM

A Report on

Gallium Interactions with Zircaloy Cladding

Ron R. Hart, John Rennie, Kevin Aucoin, Mike West
Texas A&M University
College Station, Texas

Kenan Ünlü, Carlos Ríos-Martínez
The University of Texas at Austin
Austin, Texas

Submitted for publication to

Amarillo National Resource Center for Plutonium

May 1998

TABLE OF CONTENTS

List of Figures.....	v
Introduction.....	1
Experimental Procedure	3
Results and Discussion.....	5
Conclusion.....	15
Acknowledgments.....	16
References.....	17

LIST OF FIGURES

Figure 1 - 200 keV Accelerator.....	3
Figure 2 - Target Holder and Heater Assembly.....	4
Figure 3 - SEM Micrographs of Zircaloy-IV.....	5
Figure 4 - Ga-K and Ga-L X-Ray Map.....	6
Figure 5 - Backscattered Energy Spectra.....	8
Figure 6 - SIMS Analysis of Zircaloy-IV	10
Figure 7 - SIMS Analysis of Zircaloy-IV	11
Figure 8 - SIMS Analysis of Zircaloy-IV	12

Gallium Interactions with Zircaloy Cladding

Ron R. Hart, John Rennie, Kevin Aucoin, Mike West (Texas A&M University)

Kenan Ünlü, Carlos Ríos-Martínez (The University of Texas at Austin)

The effects of Ga from weapons-grade plutonium MOX fuel on zircaloy-IV cladding during power reactor operation have been simulated by implantations of 100 keV Ga-69 ions into a polished zircaloy-IV sample while the sample was maintained at a typical cladding temperature of 375°C. Analyses were based on scanning electron microscopy, Rutherford backscattering of 280 keV He-3 ions, and secondary ion mass spectroscopy. Subgrains at the zircaloy-IV surface formed at a Ga fluence equivalent to total release of approximately 12 ppm by weight of Ga from the fuel. The subgrains may be an intermetallic compound of Zr_2Ga . Enhanced diffusion of Ga was observed, but Ga concentrations decreased 3 orders of magnitude over a depth of 3000 Å.

Introduction

The currently accepted approaches for the disposition of weapons-grade plutonium in the U.S. include both immobilization and mixed oxide (MOX) fuel conversion options. MOX fuels from the processed spent fuels of light-water reactors (LWRs) have been used in Europe during the last three decades, and the performance and cladding compatibility of these fuels have been studied extensively. However, there is no data available about the possible effects of the MOX fuel converted from weapons-grade plutonium on fuel performance and cladding compatibility. Since the U.S. weapons-grade plutonium has small amounts of gallium,¹ which may be partially incorporated into the MOX fuel during

fabrication, the effects of this reactive element on fuel components need to be understood before using these fuels commercially.

Currently, there are ongoing studies at the National Laboratories to clarify some of the issues regarding gallium.² We are presently investigating the effects of gallium from weapons-grade plutonium MOX fuel on cladding materials, particularly zircaloy, during simulated reactor irradiation. The methodology used for this study and some preliminary observations are presented in this paper.

Although the precise chemical form of gallium in MOX fuel is not known,²⁻⁴ one can assume that gallium is present in either elemental or oxide form (Ga_2O_3).⁵ In any event, the Ga released from the pellet will interact with the cladding while the cladding is also being irradiated with fission fragments, neutrons, beta particles, and gamma rays. Of the radiation released during the fission process, fission fragments are the primary concern since they produce a high density of atomic displacements in the surface region of the cladding. The vacancies and interstitials thus produced may interact with Ga atoms which reach the surface of the cladding from the fuel. Consequently, enhanced diffusion of the Ga or possibly enhanced chemical reactions may occur during reactor irradiation.⁶ If gallium is present as an oxide, the irradiation conditions will probably lead to breakup of the molecule, so that Ga may still diffuse into the cladding. Clearly, the Ga-cladding interaction will not be under thermal equilibrium conditions.

It is estimated that each ppm by weight (wppm) of Ga in the MOX fuel, if released through the radial boundary of a fuel pellet, would lead to a fluence of 2.4×10^{16} Ga atoms/cm² that impact the inner surface of the cladding. It is presently anticipated that processes used in the fabrication of the weapons-grade Pu MOX fuel will result in a Ga content in the fuel of about 10 wppm.² This amount of Ga corresponds to a fluence of 2.4×10^{17} Ga atoms/cm².

Experimental Procedure

To approximately simulate a power reactor environment, Ga-69 ions were implanted to fluences in the 10^{16} to $10^{18}/\text{cm}^2$ range into a polished zircaloy-IV sample to a shallow depth of about 400 \AA (100 keV ions) while the sample was maintained at a typical cladding temperature of 375°C . Calculations using the TRIM code give a projected range of 409 \AA and a standard deviation in projected range of 229 \AA .⁷ The Ga implantations also produce displacement effects over the projected range similar to those produced by fission fragments. At a typical power density of 300 W/cm^3 in the fuel it is estimated that, neglecting ion beam sputtering, a fluence of $3 \times 10^{17}/\text{cm}^2$ of 100 keV Ga ions will produce the same density of lattice displacements over their projected range as will the fission fragments in about 1 year of power reactor operation.

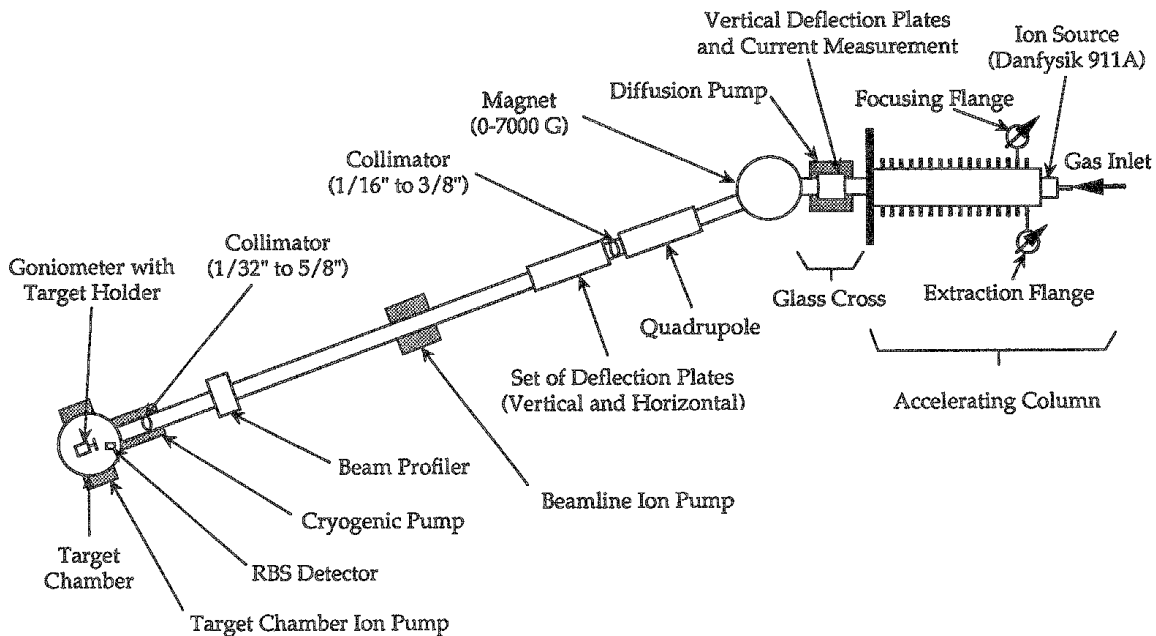


Figure 1: 200 keV Accelerator

Figure 1 is a schematic of the 200 kV accelerator used for this work. Ga ions were produced using an oven assembly to evaporate Ga atoms into the discharge region of a hollow cathode ion source. After extraction and focusing the ion beam was accelerated to

ground potential and then magnetically deflected by 20 degrees for mass separation of Ga-69. The ion beam was then transmitted to the target chamber where it was collimated to 1/8 inch diameter before striking the target at normal incidence.

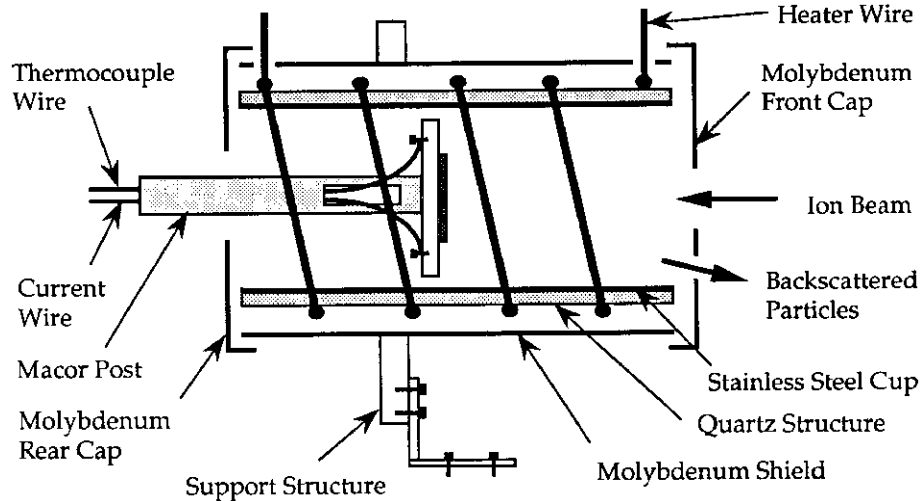


Figure 2: Target Holder and Heater Assembly

Figure 2 is a schematic of the target holder and oven heating assembly. A thermocouple attached to the target holder was used to monitor target temperature and provide electrical connection for the measurement of target current. A stainless steel inner liner of the oven was biased at a negative voltage of 200 V to suppress secondary electron emission from the target. The vacuum level of the target chamber was less than 10^{-7} torr during the implantations.

After cooling to room temperature the implanted areas, as well as an unimplanted area, were analyzed by in situ Rutherford backscattering analyses using 280 keV doubly-ionized He-3 ions. A solid state detector was located at a scattering angle of 160° for detection of the backscattered He-3 ions. Subsequently, the sample was analyzed using scanning electron microscopy (SEM) at the Electron Microscopy Center at Texas A&M University, electron microprobe analyses at the Department of Geology at Texas A&M University, and secondary ion mass spectroscopy (SIMS) at Charles Evans and Associates, Inc.⁸

Results and Discussion

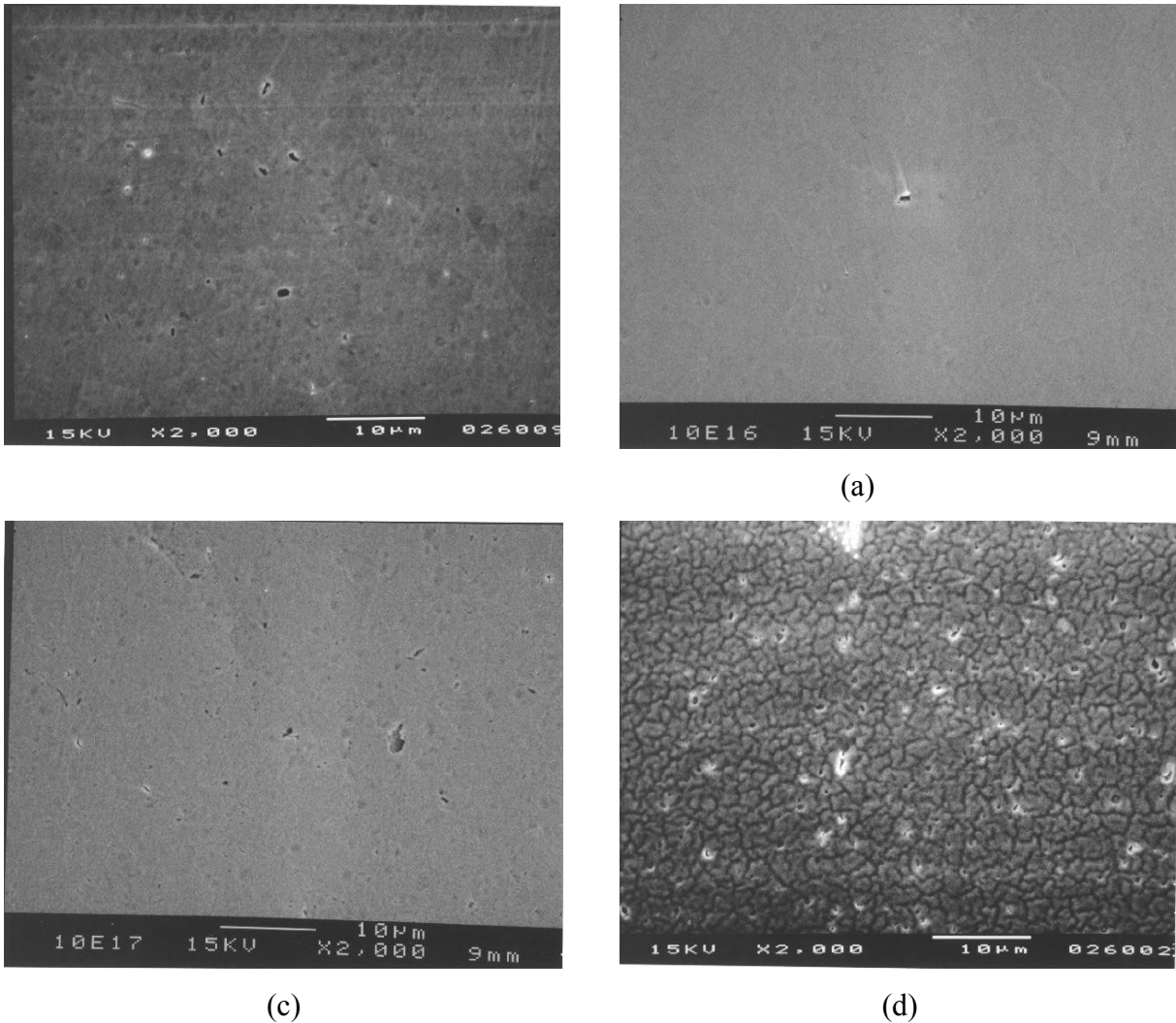


Figure 3: SEM Micrographs of Zircaloy-IV following Implantations of 100 keV Ga Ions to Varying Fluences. The sample was maintained at a temperature of 375 °C during the implantations. (a) unimplanted, (b) 10^{16} ions/cm², (c) 10^{17} ions/cm², and (d) 10^{18} ions/cm².

Figure 3 shows SEM micrographs of the sample surface of an unimplanted area as well as implanted areas with fluences of 10^{16} , 10^{17} , and 10^{18} Ga ions/cm². No significant differences can be seen between the unimplanted area and the areas with fluences of 10^{16} and 10^{17} /cm². In particular, there are no observable effects, such as blisters, pits, etc., up to a fluence of 10^{17} /cm² that are not present on the unimplanted area. However, the area

implanted with $10^{18}/\text{cm}^2$ shows a granular structure with grain sizes of about $2\ \mu\text{m}$. Although not shown, a high resolution SEM micrograph of the original zircaloy-IV sample showed grain sizes of $30\text{-}50\ \mu\text{m}$. Thus, these $2\ \mu\text{m}$ subgrains are not grains of the as-fabricated sample.

A micrograph from electron microprobe analysis of the area implanted with $10^{18}/\text{cm}^2$ is shown in Figure 4. An x-ray map of Ga-K and Ga-L x-rays is superimposed on a backscattered electron image of the surface. This micrograph indicates that the Ga is

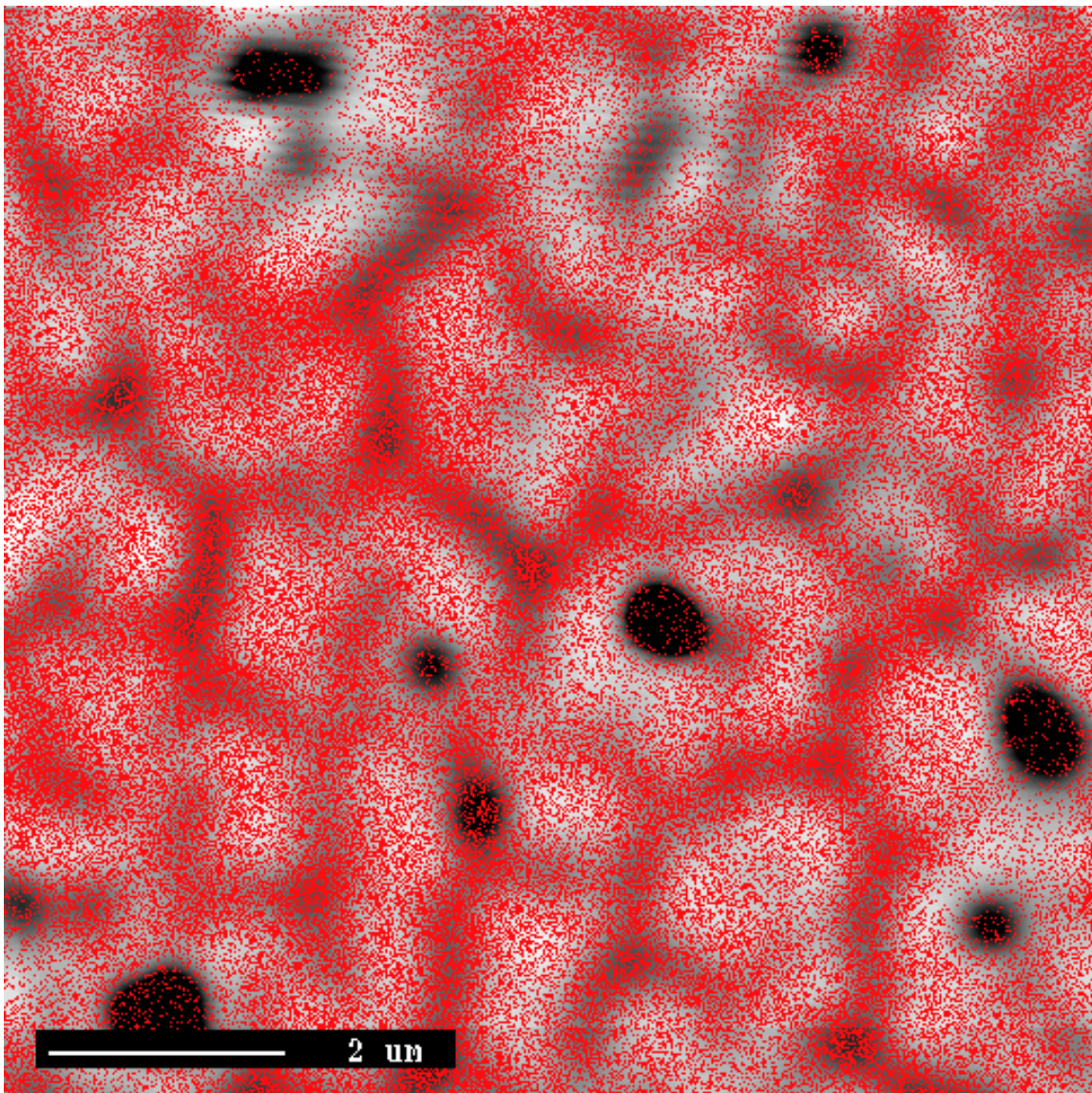


Figure 4: Ga-K and Ga-L X-Ray Map (Red Dots) Superimposed on a Backscattered Electron Image of a Zircaloy-IV Sample Implanted at $375\ ^\circ\text{C}$ with $100\ \text{keV}$ Ga Ions to a Fluence of $10^{18}\ \text{ions}/\text{cm}^2$.

not distributed uniformly. Ga is present at a high concentration in the subgrains but has a somewhat higher concentration between the subgrains. Note that the spatial resolution for electron microprobe analysis is about $1 \mu\text{m}^3$; thus, the Ga distribution across the surface is not precisely determined by this micrograph. The dark spots seen in Figure 4 are caused by surface blemishes which can also be seen on the unimplanted area.

Backscattered energy spectra of 280 keV He-3 incident on the 10^{17} and $10^{18}/\text{cm}^2$ implants, as well as on an unimplanted area, are shown in Figure 5. First consider the spectrum from the unimplanted area. The edge at a channel number of 725 corresponds to a backscattered energy of 246 keV from Zr atoms on the surface. The increasing yield at lower backscattered energies is caused by backscattering from Zr atoms at increasing depths within the target and is due to the $1/E^2$ dependence of the Rutherford backscattering cross-section. Based on the energy-dependent stopping power from the TRIM code, the depth scale is $10.6 \text{ \AA}/\text{keV}$ or $360 \text{ \AA}/100$ channels. The slope of the Zr edge gives a depth resolution of about 100 \AA .

Now considering the $10^{17}/\text{cm}^2$ implant, which is equivalent to a Ga content in the fuel of 4 wppm, it can be seen that the backscattered yield near the surface is depressed relative to the yield from the unimplanted area. The fractional decrease is 26% which implies that approximately 26% of the Zr atoms have been replaced⁹ with Ga atoms. The Ga alters the depth scale to $11.6 \text{ \AA}/\text{keV}$ or $394 \text{ \AA}/100$ channels. Correcting for the change in depth scale, the Ga fraction is increased to 28%. The Ga concentration is approximately uniform over a depth of 350 \AA and extends to a depth of about 650 \AA . These depths are in reasonable agreement with the predicted projected range of 409 \AA and the sum of the projected range plus one standard deviation in projected range of 638 \AA .

The backscattered energy spectrum from the $10^{18}/\text{cm}^2$ implant indicates that the Ga fraction near the surface has increased to 39% with a depth scale factor of $405 \text{ \AA}/100$

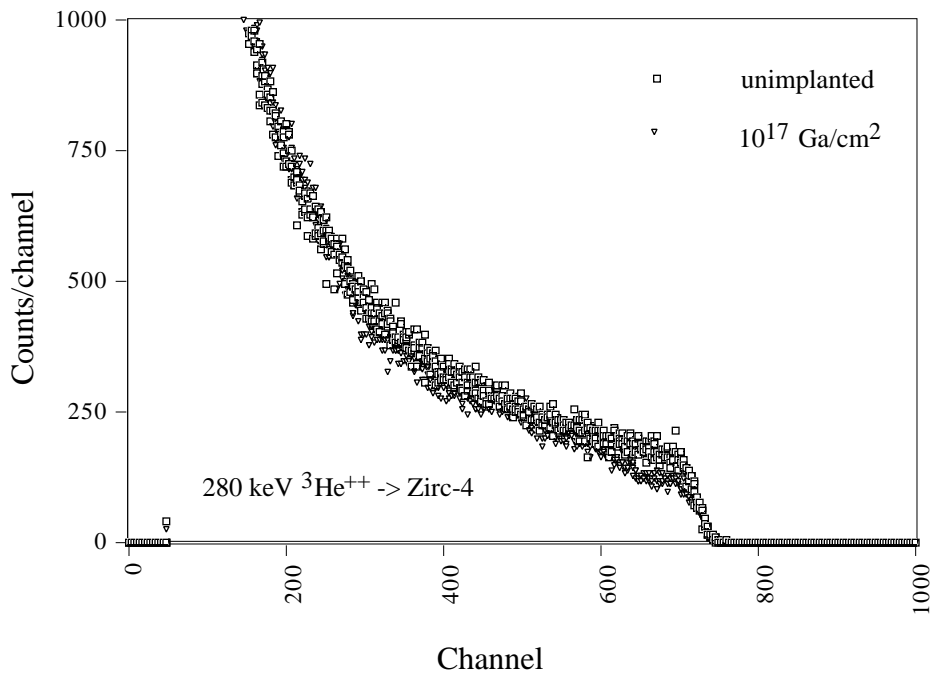
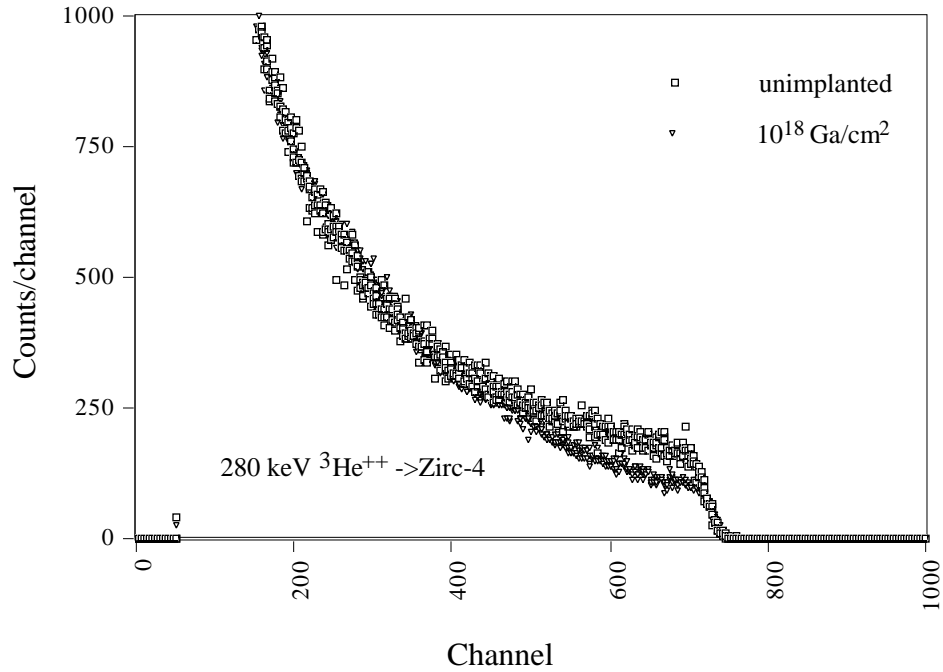


Figure 5: Backscattered Energy Spectra of 280 keV He-3 Incident on Zircaloy-IV Implanted at 375 $^{\circ}\text{C}$ with 100 keV Ga to Fluences of 10^{17} and $10^{18}/\text{cm}^2$. In each case a spectrum from an unimplanted area is also shown.

channels. The Ga is again approximately constant for several hundred Å near the surface but extends to the relatively deep depth of about 1100 Å. This deep penetration is probably caused by enhanced diffusion due to the vacancies produced during the implantation. In comparing the spectra from the 10^{17} and $10^{18}/\text{cm}^2$ implants it is apparent that not all of the Ga implanted into the sample during the $10^{18}/\text{cm}^2$ implant was retained in the sample, but rather only about a factor of 3 more than that of the $10^{17}/\text{cm}^2$ implant. This loss of Ga is probably caused by the sputtering process occurring during the high-fluence implantation which leads to a saturation of Ga concentration. Consequently, the $10^{18}/\text{cm}^2$ implant is, in effect, approximately a $3 \times 10^{17}/\text{cm}^2$ implant. This fluence of Ga is equivalent to a Ga content in the fuel of about 12 wppm, which is near the 10 wppm that is presently expected in the weapons-grade Pu MOX fuel.

SIMS data showing the Ga depth profiles for the three implanted areas are shown in Figures 6-8. Note that the ordinates are only approximate. The emphasis is on the shape of the Ga profiles after the sputtering process during analysis has come to equilibrium. Neglecting a transition depth of about 100 Å at the surface, the 10^{16} ions/ cm^2 implant shows a typical depth profile expected for ion implantation, i.e. a peak near the projected range of 409 Å and a Gaussian-like tail that decreases to $1/e$ of the peak concentration at a depth of about 650 Å, which corresponds to the calculated projected range plus one standard deviation in projected range of 638 Å. The $10^{17}/\text{cm}^2$ implant has a similar shape, but, as expected, the peak concentration is about an order of magnitude greater. The advantage of SIMS is its high sensitivity. Consequently, the Ga profile can be followed down to three orders of magnitude below the peak concentration; this occurs at a depth of about 2000 Å. Since the $10^{17}/\text{cm}^2$ implant results in a similar shape as the shape of the Ga profile of the $10^{16}/\text{cm}^2$ implant, there appears to be no significant enhanced diffusion of the implanted Ga. Since the RBS data for the $10^{17}/\text{cm}^2$ implant indicates an approximately flat

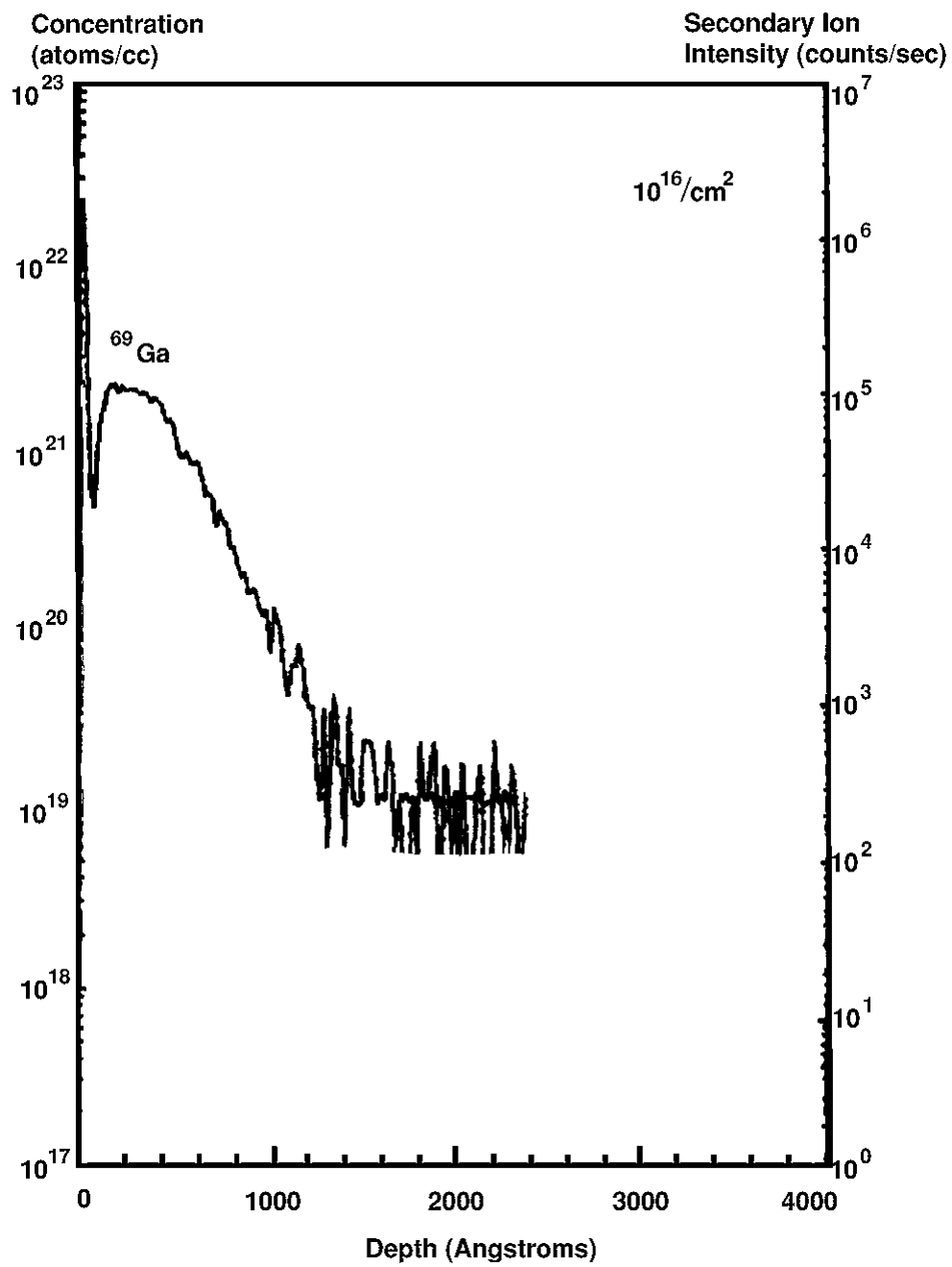


Figure 6: SIMS Analysis of Zircaloy-IV Implanted at 375 °C with 100 keV Ga to a Fluence of $10^{16}/\text{cm}^2$

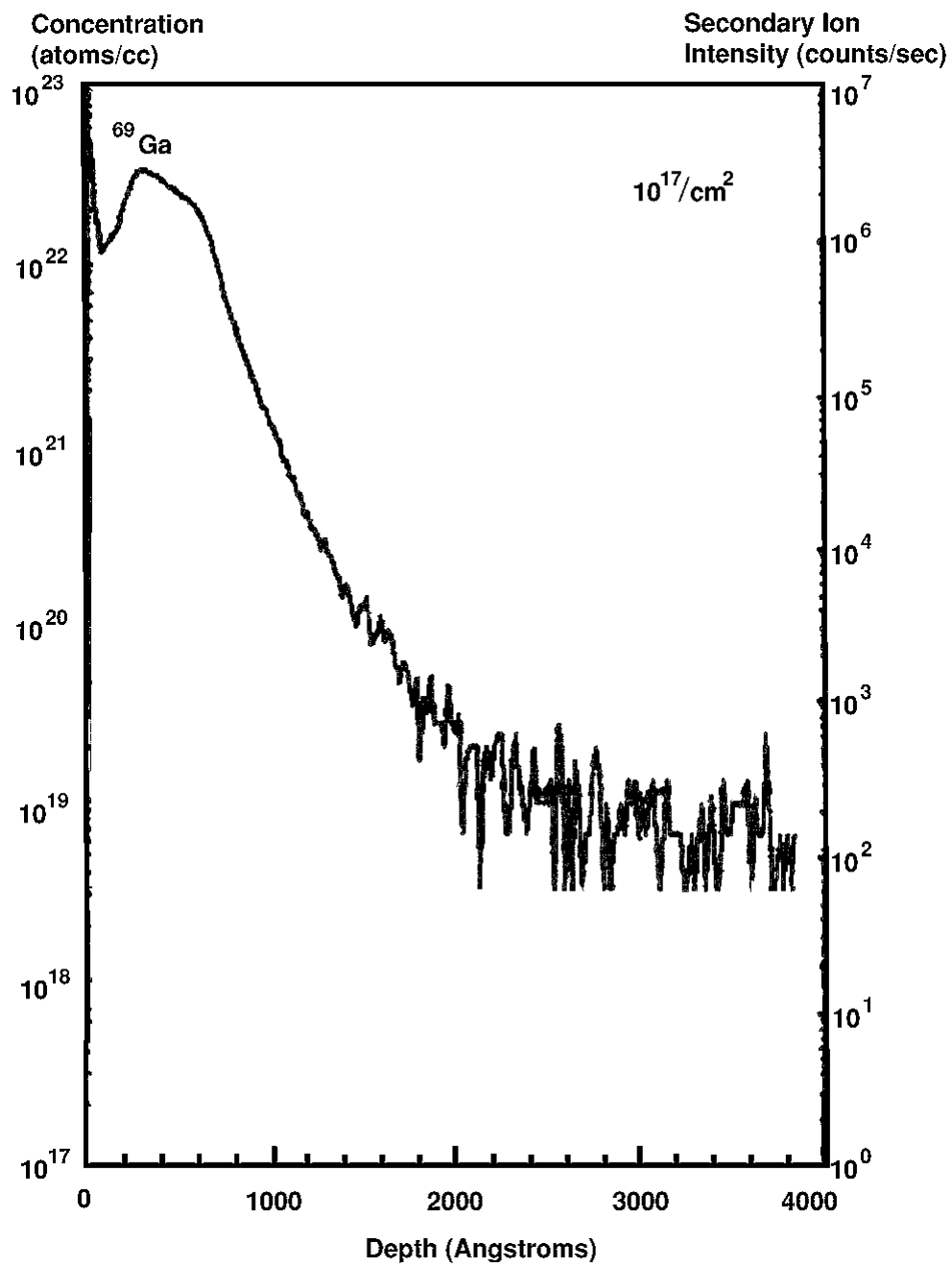


Figure 7: SIMS Analysis of Zircaloy-IV Implanted at 375 °C with 100 keV Ga to a Fluence of $10^{17}/\text{cm}^2$

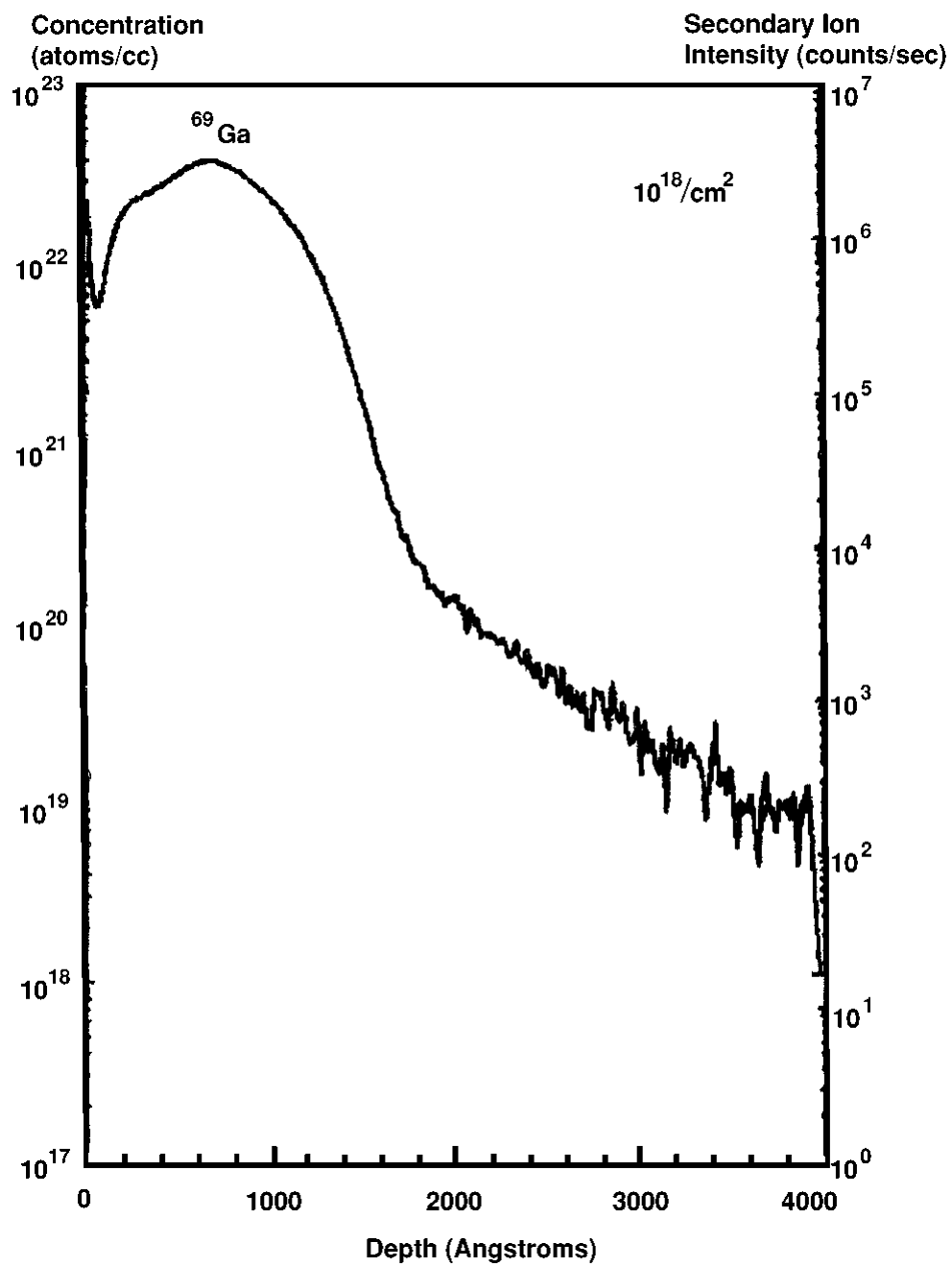


Figure 8: SIMS Analysis of Zircaloy-IV Implanted at 375 °C with 100 keV Ga to a Fluence of $10^{18}/\text{cm}^2$

Ga profile over a depth of 350 Å, the SIMS results may reflect a greater transition depth of perhaps 200-400 Å for this implant.

The $10^{18}/\text{cm}^2$ implant gives a Ga depth profile that is significantly different from the lower fluence cases. It is apparent that the Ga concentration has approximately saturated at a value somewhat greater than the maximum of the $10^{17}/\text{cm}^2$ implant. This agrees with the RBS results. In contrast to the approximately constant depth profile over several hundred Å seen by RBS, the SIMS data again shows a Ga concentration that increases with depth at shallow depths. This may also reflect an approximately 400 Å transition depth. In agreement with the RBS results, the bulk of the Ga now penetrates to considerably deeper depths than indicated by the Ga profile of the $10^{17}/\text{cm}^2$ implant. Roughly, the bulk of the Ga penetrates 500 Å deeper for the $10^{18}/\text{cm}^2$ implant. This deeper penetration is probably caused by enhanced diffusion due to the ion beam irradiation. The Ga concentration is three orders of magnitude less than the peak concentration at a depth of about 3000 Å. If the Ga concentration continues to decrease at the same rate as the slope of the penetrating tail, the Ga content in the zircaloy will be less than 1 ppm atomic at a depth of about 6000 Å.

Conclusion

The results thus far indicate the following tentative model. Ga emitted from a fuel pellet of weapons-grade Pu MOX to zircaloy-IV cladding during power reactor operation will probably be incorporated into the cladding in solid solution up to a Ga fraction of at least 28%, corresponding to the $10^{17}/\text{cm}^2$ implant. If the Ga fraction reaches a level greater than 1/3, which occurs for the $10^{18}/\text{cm}^2$ implant, an intermetallic compound of Zr_2Ga may form. This is the lowest Ga fraction intermetallic compound indicated on the Ga-Zr phase diagram.² This compound may produce the subgrain ($\sim 2 \mu\text{m}$) regions seen following the $10^{18}/\text{cm}^2$ implant, which, at ion-sputtering-induced saturation, corresponds to total release of about 12 wppm of Ga in the fuel. Such a compound should be quite stable at typical cladding temperatures. Ga in excess of that needed to form Zr_2Ga may be rejected from the intermetallic compound phase and relatively easily diffused by enhanced diffusion through the $\sim 10 \mu\text{m}$ depth of the range of fission fragments in the cladding. Penetration beyond this depth may be on the order of $1 \mu\text{m}$.

In summary, Zr_2Ga subgrain crystallites may form on the surface where Ga concentration is high; a much lower concentration of Ga may be present in solid solution to a depth somewhat greater than $10 \mu\text{m}$. It should be emphasized that the results and tentative model are based on an unstressed zircaloy sample but, nevertheless, are encouraging for the possible use of weapons-grade Pu MOX in power reactors using anticipated Pu conversion processes. Additional work in progress will aid in the possible confirmation of this model.

At this point the possibility of liquid metal embrittlement cannot be ruled out.² However, the micrograph shown in Figure 4 did not indicate extra Ga at original grain boundaries but only between subgrains. Neither can the possibility of a synergism between fission fragments of Cd, which lead to reduced ductility, and Ga be eliminated.² Further work is required to study these concerns.

Acknowledgments

The assistance of Dr. Bill Moddeman, Pantex, in obtaining the SIMS data is greatly appreciated.

This study was performed with the support of the U.S. Department of Energy, Cooperative Agreement No. DE-FC04-95AL85832. However, any opinions, findings, conclusions or recommendations expressed herein are those of the authors and do not necessarily reflect the views of DOE. This work was conducted through the Amarillo National Resource Center for Plutonium.

References

1. T. B. Lindemer, "Assessment of Gallium Effects in Processing and Performance of U-Pu Oxide LWR Fuels," Oak Ridge National Laboratory, Fissile Materials Disposition Program, ORNL/MD/LTR-38.
2. Dane F. Wilson, Edward C. Beahm, Theodore M. Besmann, Jackson H. DeVan, James R. DiStefano, Uri Gat, Sherrell R. Greene, Phillip L. Rittenhouse, Brian A. Worley, "Potential Effects of Gallium on Cladding Materials," Oak Ridge National Laboratory, ORNL/TM-13504.
3. Nuclear Fuels Technologies, Gallium Evaluation Test Plan, Fissile Materials Disposition Program, Los Alamos National Laboratory, Report No: LA-UR-96-920.
4. Nuclear Fuels Technologies, Fiscal Year 1996 Research and Development Test Matrices, Fissile Materials Disposition Program, Los Alamos National Laboratory, Report No: LA-UR-96-856.
5. I.A. Sheka, L.S. Chaus, and T.T. Mutyevera, *The Chemistry of Gallium*, Elsevier, (1996).
6. M. Gettings, K. G. Langguth, and G. Linker, "Radiation Damage and Ion Behavior in Ion Implanted Vanadium and Nickel Single Crystals," *Applications of Ion Beams to Metals*, edited by S. T. Picraux, E. P. EerNisse, and F. L. Vook (Plenum Press, New York, 1974) p. 241.
7. J. F. Ziegler, J. P. Biersack and U. Littmark, *The Stopping and Range of Ions in Solids* (Pergamon, New York, 1985).
8. The SIMS analysis was performed under the supervision of Dr. Bill Moddeman, Pantex.
9. H. J. Smith and G. N. Van Wyk, "Anomalous Room Temperature Diffusion of Ion-Injected Ni in Zn Targets," *Applications of Ion Beams to Metals*, op. cit., p. 295.